Available online at www.sciencedirect.com

ScienceDirect

Procedia CIRP 99 (2021) 336–341

www.elsevier.com/locate/procedia

14th CIRP Conference on Intelligent Computation in Manufacturing Engineering, CIRP ICME '20

Residual stress investigation on Ti-48Al-2Cr-2Nb samples produced by Electron Beam Melting process

Manuela Galati[a,*], Giovanni Rizza[a], Alessandro Salmi[a], Sara Biamino[b], Cristian Ghibaudo[b], Paolo Fino[b], Luca Iuliano[a]

[a]*Department od Management and Production Engineering (DIGEP), Politecnico di Torino, Corso Duca degli Abruzzi 24, 10129 Torino, Italy*
[b]*Department of Applied Science and Technology (DISAT) Politecnico di Torino, Corso Duca degli Abruzzi 24, 10129 Torino, Italy*
* Corresponding author. Tel.: +390110904569. *E-mail address:* manuela.galati@polito.it

Abstract

Ti-48Al-2Cr-2Nb (Ti-48-2-2) is an intermetallic alloy belonging to a family of gamma-TiAl intermetallic alloys that are attracting significant attention. Electron Beam Melting (EBM) process is today the only manufacturing process that allows effective production of parts made by these kinds of alloys. Proper process control avoids high temperatures in the surrounding areas that may generate significant residual stresses that could cause micro-cracks. In this paper, an investigation on the residual stress state on Ti-48-2-2 parts is carried out using the hole drilling method. In particular, the influence of EBM process parameters is evaluated in order to understand the effects of the residual stresses on part integrity.

Peer-review under responsibility of the scientific committee of the 14th CIRP Conference on Intelligent Computation in Manufacturing Engineering, 15-17 July 2020.

Keywords: Intermetallic alloy, cracks, Hole drilling method, Additive manufacturing

1. Introduction

The intermetallic compounds such as Ti-48Al-2Cr-2Nb are fascinating materials because they are characterized by specific mechanical properties comparable to the superalloys one coupled with a low density. These properties make this kind of alloy perfectly suitable for aeronautical and automotive applications [1,2], in which the ratio between the mechanical properties and the component weight plays a key role. However, the positive aspects of these alloys come with the drawbacks of reduced ductility and fracture toughness. These properties could also get worse if residual thermal stresses are induced in the component during the process. Residual stresses are a crucial issue for components produced with AM techniques. These could induce internal cracks, delamination, loss of shape, and low dimensional accuracy [3]. Although the components produced with AM techniques generally require finishing operations, if the induced deformations are large, the finishing operations may not generate an accurate component.

Moreover, residual stresses are found to have a deep influence on the crack growth and fatigue properties of the components. [4,5] The origin of residual stresses is identified in a significant thermal gradient or a differential cooling.[3,6–8]. Because of that, this kind of alloys needs to be processed in a warm environment so that the thermal gradient is low. For such reason, Electron Beam Melting (EBM), an Additive Manufacturing (AM) technique, is today the only capable of producing functional components made by intermetallic alloys. EBM uses an electron beam to selectively melt a metallic powder bed according to the cross-section of the component to build. The material is directly heated by the power of the electron beam and undergoes thermal expansion. However, after the beam passage, the rapid heat transfer towards the surrounding material cools down the melted area rapidly. At the next beam passage, the beam melts a line adjacent to the previous one. To ensure the welding between adjacent lines, the beam track overlaps the previous melted line partially. This causes thermal cycles in the material that, in turn, involve rapid cycles of the expansion and shrink. During the cooling phase, the

Peer-review under responsibility of the scientific committee of the 14th CIRP Conference on Intelligent Computation in Manufacturing Engineering, 15-17 July 2020.
10.1016/j.procir.2021.03.049

shrinkage of the material is partially constrained by the plastic deformation created during the previous heating phase [3]. Thanks to the high working temperature in the chamber [9,10], the temperature gradients of the molten state and the surrounding material are reduced, and, therefore, the residual stresses are lower. Additionally, at the end of the process, the entire build is cold down in the EBM chamber and within low helium[11]. The cooling phase is a long process phase. The higher is the temperature in the chamber and the size of the build, the longer will be the cooling time. This low cooling acts as a stress-relieving treatment that reduces residual stresses.

For this reason, it is widely accepted that residual stresses in components produced with EBM are low [12–14]. Sochalski-Kolbus et al. [7] compared the residual stresses of Inconel 718 parts produced by EBM and laser beam powder bed fusion process (LB-PBF). The residual stresses of the component produced by EBM were an order of magnitude smaller than the one produced by LB-PBF. For EBM, the average tensile stresses along z-direction (building direction) and in x-direction were 21 MPa and 22 MPa, respectively. Several studies highlighted that for the LB-PBF techniques, process parameters have a great influence on residual stresses [3,5,15]. Although this influence is evident for LB-PBF techniques, since the common belief of low residual stresses, they are rarely measured for components made by EBM technique. Therefore, a literature gap exists in this field.

Additionally, as for LB-PBF, the process parameters play a crucial role in the residual stresses, especially when they create a strong thermal gradient between the melt pool and the surrounding material [16]. This work aims to investigate the presence of residual stresses in Ti-48Al-2Cr-2Nb samples produced by EBM. The influence of process parameters is also investigated. The hole drilling method is adopted to evaluate the residual stresses present on the top and the lateral surfaces of the samples.

2. Material and methods

As mentioned above, the material considered in this work is Standard Arcam Ti-48Al-2Nb-2Cr. Samples have been produced varying the beam current, line offset, and scan speed. From the main parameters, secondary indicators have been derived as indicators of the process efficiency, such as the line energy and the area energy [9]. The exact parameters are reported in Table 1. The process parameters combinations were indexed in alphabetic order and coupled to analyze the effect of each process parameters as follows:

- A and C, effects of the beam current
- C and D, effects of line offset
- B and C, the effect of the scan speed

Additionally, samples A and B have the same line and area energies.

2.1. Sample production

An Arcam A2X system has been used to produce one sample for each process parameters combination. The samples were parallelepipeds with a cross section of 18x18 mm^2 and height equal to 30 mm. The samples were attached directly to the building platform. Before to start the process, the building platform was heated up to 1100 °C. The same temperature was set for the preheating of each layer. The layer thickness was set to 0.09 mm. The melting strategy consisted of unidirectional parallel lines with a clockwise rotation of 90 degrees every layer. No contour has been used. The time to produce the sample was around 12 hours, including the cooling time. After the production, the samples have been cleaned from loose powder by blasting and using the same powder of the process.

Table 1. Process parameters.

Sample	Beam current [mA]	Line offset [mA]	Scan speed [mm/s]	Line energy [J/mm]	Area energy [J/mm^2]
A	7	0.2	1200	0.35	1.75
B	9	0.2	1542	0.35	1.75
C	9	0.2	1200	0.45	2.25
D	9	0.3	1200	0.45	1.50

2.2. Residual stresses measurements

The MTS3000 (SINT Technology s.r.l, Italy) system was used to evaluate residual stresses using the hole-drilling strain-gauge method. The relaxed deformation was measured using a K-RY61-1.5/120R (HBM Italia s.r.l., Italy) Type B 3-element rosette, in which each strain gauge was connected to a DQ430 espressoDAQ (HBM Italia s.r.l., Italy) USB amplifier in a half-bridge configuration. The RSM 7 (SINT Technology s.r.l, Italy) software package was used to control the system and the test procedure as well as to acquire the relaxed deformations. Incremental hole-drilling tests were carried out by executing 24 drilling steps to a depth of 50 μm, in compliance with the ASTM E837-13a standard; the relaxed deformations were acquired at the end of each increment with a delay of 10 seconds in order to obtain a more stable signal and setting an acquisition length for averaging of 5 seconds. The acquired surface deformations were then post-processed by EVAL 7 software (SINT Technology s.r.l, Italy), and the residual stress profile was back calculated.

The top and lateral surfaces of the specimens were prepared by polishing them with silicon carbide paper (200 and 400 grit) in order to meet the exact bonding roughness requirements (2-4 μm). Before gluing the rosette, the surface was cleaned using a mixture of acetone and isopropanol. The rosette was then bonded using Z70 (HBM Italia s.r.l., Italy) cold curing superglue. Three measurements were performed for each sample. On the top surface, the strain gage rosette was installed in order to locate the centre of the grid pattern at the center of the surface. On the vertical surfaces with the normal parallel to the rake movement, strain gage rosettes were installed in order to locate the centre of the grid pattern along the vertical centreline (℄) of the face and at $z = 5$ mm and $z = 25$ mm, respectively, from the bottom surface (the surface that was in contact with the build platform).

Consequently, the distance between the adjacent holes and from the free edges complied with the geometrical specifications extrapolated from the ASTM E837-13a standard [17]. Fig. 1 shows the experimental setup configuration.

2.3. Microstructure

The samples were cut along the building direction, grounded with SiC paper and then polished down to 1µm with diamond paste. Porosity analysis was conducted by image analysis on the polished specimens with ImageJ on 10 images, according to the ASTM-E2109. The samples were etched with Kroll's solution for 5 seconds. Both porosity and microstructure images were obtained by Leica DM optical microscope (5000ILM).

3. Results

3.1. Residual stresses measurements

Fig. 2 depicts the residual stress profiles in terms of the principal stresses and the direction of the maximum principal stress on the top and on the lateral surfaces of the samples.

Fig. 2(a) shows the residual stress depth profile of sample A. The residual stress state on the top surface is positive and ranges between zero and 50 MPa except for the depth close to 1 mm, where the material is under slight compression. Oscillating behavior is noticeable from a depth of 0.5 mm. Residual stresses on the lateral surfaces are higher than ones on the top and are characterized by a more pronounced oscillating behavior. The lateral residual stresses measured at $z = 25$ mm are on average higher than the ones measured on the top and exhibit a moderate compression at depth ranges from 0.35 mm to 0.55 mm; at a depth higher than 0.9 mm, the values at the top and the lateral surfaces are similar. At $z = 5$ mm, the lateral surface shows almost tensile stresses and an increasing trend along with the depth up to 130 MPa. The direction of the maximum principal stress, β, is quite variable but similar for all the three measurement positions, especially for depth ranges from 0.4 mm and 0.8 mm. A shift of 0.15 mm could be observed for the lateral measurement at $z = 5$ mm, probably due to a combination of zero offset error and sample preparation.

The residual stress depth profile of sample B is shown in Fig. 2(b). The top surface exhibits a maximum tensile state of 100 MPa to a depth of about 0.1 mm from the surface. After a gradual increase, an almost uniform tensile stress of about 25 MPa is observed from a depth of 0.45 mm. Residual stresses on the lateral surface close to the build platform are around 30 MPa and uniform through the thickness up to a depth of 0.4 mm then rapidly increase up to 215 MPa with a maximum at a depth of 0.7 mm. At higher depth, an oscillating trend is observed with a maximum tensile stress of about 180 MPa at the deepest point. Similar to sample A, residual stresses on the lateral surface close to the top surface exhibit higher initial tensile stresses, then they became quite uniform with a maximum tensile stress of about 60 MPa, whereas a steep increase is observed from a depth of 0.8 mm.

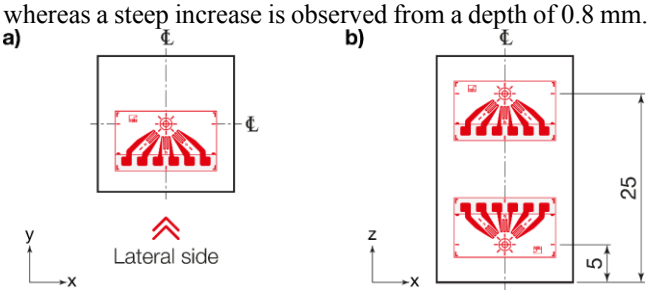

Fig. 1. Experimental setup for the residual stress measurements and positions of the rosette for (a) the top surface and for (b) the lateral surface

From a depth of 0.85 mm, the magnitude of the stresses is quite similar to the ones close to the build platform. Even in this case, the β angle is not uniform. Measurements on top and the lateral surface close to the top exhibit similar behavior just beneath the surface and in depth.

Fig. 2(c) shows the stress profiles measured in sample C. Uniform tensile stress of 25 MPa is observed on the top surface at a depth of between 0.15 mm and 0.55 mm. Then stresses slightly increase up to 50 MPa and remains uniform from a depth of 0.8 mm. On the lateral surface at $z = 5$ mm, the subsurface stress values are comparable with ones on the top. A low compressive stress of about 20 MPa is observed at depth ranges from 0.15 mm to 0.25 mm. Then the stress increases with some oscillation up to 260 MPa at the maximum depth. Analogously to the previous cases, higher subsurface tensile stresses are observed at $z = 25$ mm, while a uniform stress state is observed up to a depth of 0.5 mm, then the oscillating trend increases and can be appreciated especially from a depth of 0.85 mm. This behavior is like one of sample B. A periodic oscillating behavior of β angle between 30°-40° and 50°-60° could be observed in the case of lateral measurements. A shift similar to the one identified for sample A is also present here. The β angle on the top is mainly negative and close to 60°-80°.

Fig. 2(d) plots the stresses profiles measured in sample D. At the top surface, no significant differences can be observed with respect to sample C, except that the uniform stress behavior is more extended along the depth. Tensile residual stresses somewhat increase up to 50 MPa at the maximum depth. The stresses of the surface measure close to the build platform are comparable to the ones on the top up to a depth of 0.2 mm, while the stresses, first, linearly increase up to 130 MPa and then decrease from a depth of 0.9 mm. Lateral stresses at $z = 25$ mm are characterized by a similar behavior to sample B and C, but with reduced increase trend. No specific trend of the direction of the maximum principal stress could be identified for measures on the top and on the lateral surface close to the starting plate; a periodic oscillation with a period similar to the one of sample C is exhibited for the lateral measure at $z = 25$ mm.

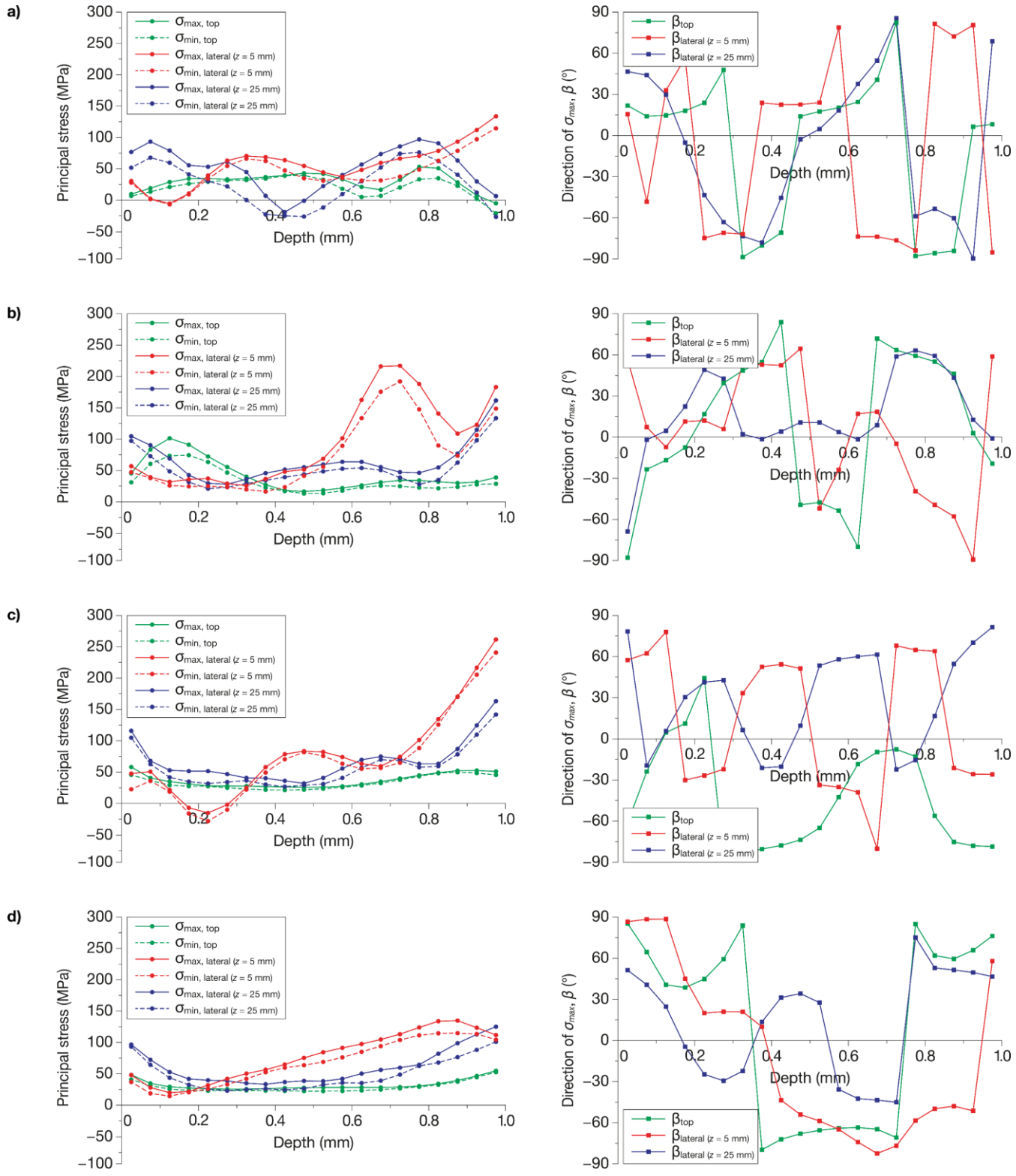

Fig. 2. Residual stresses and β measurements: (a) sample A; (b) sample B; (c) sample C; (d) sample D.

3.2. Microstructure

Generally, in the as-built EBM specimens is possible to find two types of defects, elongated pores, attributed to non-optimized parameters, and spherical pores, attributed to gas trapped during the production of powders employed during EBM component production [18]. In this work, only spherical pores were observed among all the specimens (Fig. 3). Looking at Fig 4, the average porosity of the four samples decreases with the decrease of scan speed (B and C), and with the increase line offset (C and D), while no differences are observed between samples with different beam current (A and C). Therefore, the level of porosity was considered satisfactory for all the four conditions.

As regards the microstructure, the optical microscope

characterization of the four conditions is showed in Fig. 5. For all the four conditions the typical microstructure for as-built EBM γ-TiAl components [1,19–22]was observed: the microstructure is mainly formed by two alternating bands, one formed by very fine γ and α_2 grains (duplex band) and the other by coarser equiaxed γ grains (γ-band). These bands are perpendicular to the build direction, due to the layer by layer nature of the EBM process. The as-EBM microstructure *i*s extremely fine, in comparison to the conventional processed TiAl material, as can be expected by the small melt pool and the rapid cooling experienced in the EBM process. For all the samples, the duplex band is pronounced compared to the γ-band, and trough optical microscopy, it is not possible to observe noticeable differences between the microstructure of all the samples produced in this work. It must be pointed out that this microstructure is not the final one because a heat treatment must be set up in order to reach the final desired mechanical properties. However, the as-EBM microstructure revealed can be easily transformed in all the final microstructures through the chosen heat treatment [20].

3.3. Discussion

Among the selected process parameters conditions, no significant differences in the microstructure were observed through optical microscopy. However, the residual stress measurements showed that the stress profile is in some cases significantly affected by the process conditions.

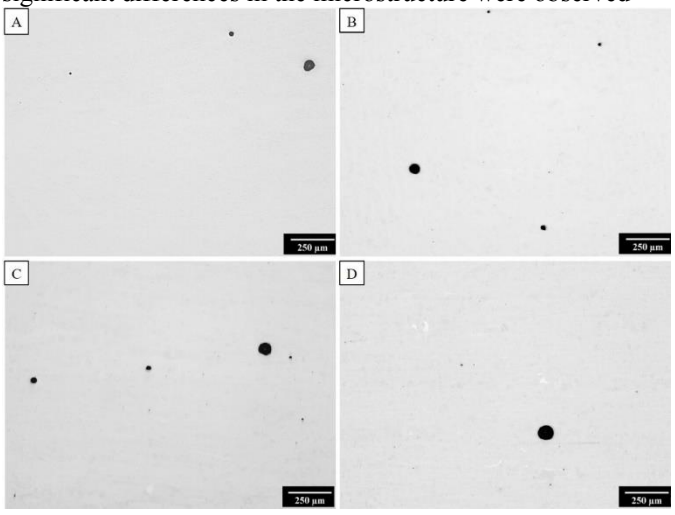

Fig. 3. Optical micrographs for porosity analysis of (A) sample A; (B) sample B; (C) sample C; (D) sample D.

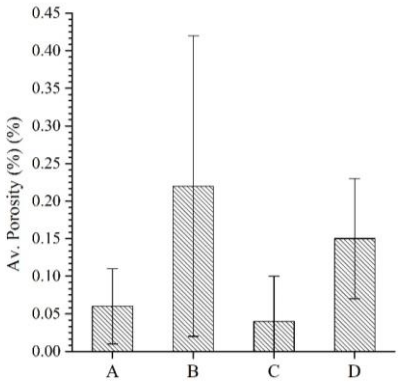

Fig. 4. Average porosity values for the sample A to D

For all the four samples residual stresses on the top surfaces are almost lower than 50 MPa and characterized by small oscillations for samples A and B, and it is quite constant for samples C and D. These low residual stress values are consistent with previous studies found in the literature on EBM parts made by Inconel 718 [7]. The lowest residual stress state on the top is observed on sample D that is characterized by a larger line offset compared to the other samples. This behavior can also be observed on a previous work on other AM parts where residual stresses were evaluated after heat treatments [23]. This analogy could be explained as an effect of the post-heating phase on the layer after the melting phase. This phase smooths the thermal gradient and makes the temperature more uniform. Then the helium, which is insufflated after the build is done, provides a typical cooling rate that could be assimilated to the one generated during a heat treatment. The different cooling rates could also explain the differences in the observed residual stresses among the top and the lateral surfaces. In details, stresses on lateral surfaces are generally higher than ones on the top and range from –25 MPa to about 250 MPa. Moreover, the residual stresses close to the bottom surface (z = 5 mm) are in general lower than residual stresses close to the bottom just beneath the surface, whereas the opposite behavior could be observed at higher depth.

A characteristic oscillating behavior, typical of parts fabricated by AM and in the case of multi-pass welding [24] is observed for samples A, B, and C. Conversely, for sample D, the oscillation is not present. A quasi-linear increasing trend could be observed for the measurements close to the starting plate and a U-shape profile, resembling the one of the top, for the measurements close to the top.

The differences in depth can be explained by the thermal gradient between the internal and external zones of the samples and the surrounding powder. Process conditions, such as in the case of the sample D, which produce a more uniform temperature in the sample, lead to low residual stress. The sample A is thermally similar to sample D,. However the smaller line offset causes a greater number of

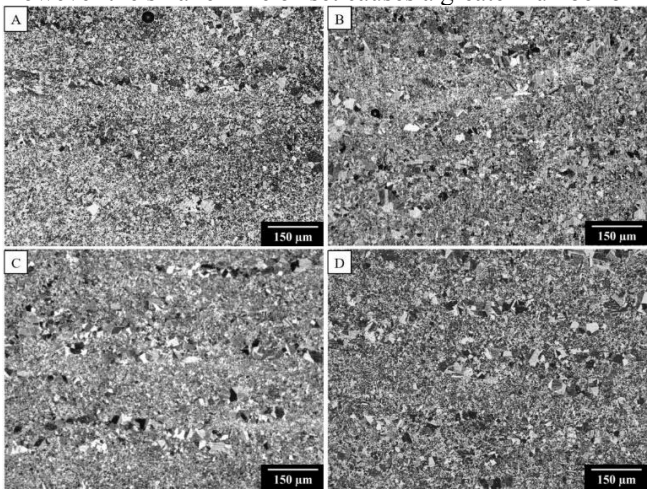

Fig. 5. Optical micrographs for microstructure investigation: (a) sample A; (b) sample B; (c) sample C; (d) sample D.

remelting phenomena and explains the more evident oscillating behavior. Similarly, the higher beam current and the low line offset involve a higher temperature in sample B and C with respect to the other and therefore a strong thermal gradient between the external and internal zones of the sample. The generated thermal gradients explain the more pronounced oscillating behavior and the higher residual stresses.

4. Conclusion

The paper investigates the correlation between the process parameters conditions and the residual stresses measured on Ti-48Al-2Cr-2Nb samples made by EBM. The microstructure analysis performed through optical microscope did not highlight a strong effect of the chosen process conditions. Conversely, the effects of the generated thermal fields due to the different process conditions can be visible in the residual stresses' measurements as well as porosities. As regards residual stresses which is the main topic of this work, thanks to the post-heating, the more uniform temperature distribution produces a low residual stress state on the top surfaces of all samples. For the lateral surfaces, the residual stresses vary along with the measuring depth and highlight that the effect of the thermal gradient between the surrounding powder, external and internal zones. This work demonstrated that also for EBM components, it is essential to evaluate the residual stresses.

References

[1] Baudana G, Biamino S, Ugues D, Lombardi M, Fino P, Pavese M, Badini C. Titanium aluminides for aerospace and automotive applications processed by Electron Beam Melting: Contribution of Politecnico di Torino. Met. Powder Rep. 2016; 193–199.

[2] Kothari K, Radhakrishnan R, Wereley NM. Advances in gamma titanium aluminides and their manufacturing techniques. Prog. Aerosp. Sci. 2012; 1–16.

[3] Li C, Liu ZY, Fang XY, Guo YB. Residual Stress in Metal Additive Manufacturing, in: Procedia CIRP, Elsevier B.V., 2018: pp. 348–353.

[4] Leuders S, Thöne M, Riemer A, Niendorf T, Tröster T, Richard HA, Maier HJ. On the mechanical behaviour of titanium alloy TiAl6V4 manufactured by selective laser melting: Fatigue resistance and crack growth performance. Int. J. Fatigue. 2013; 300–307.

[5] Shipley H, McDonnell D, Culleton M, Coull R, Lupoi R, O'Donnell G, Trimble D. Optimisation of process parameters to address fundamental challenges during selective laser melting of Ti-6Al-4V: A review. Int. J. Mach. Tools Manuf. 2018; 1–20.

[6] Prabhakar P, Sames WJ, Dehoff R, Babu SS. Computational modeling of residual stress formation during the electron beam melting process for Inconel 718. Addit. Manuf. 2015; 83–91.

[7] Sochalski-Kolbus LM, Payzant EA, Cornwell PA, Watkins TR, Babu SS, Dehoff RR, Lorenz M, Ovchinnikova O, Duty C. Comparison of Residual Stresses in Inconel 718 Simple Parts Made by Electron Beam Melting and Direct Laser Metal Sintering. Metall. Mater. Trans. A Phys. Metall. Mater. Sci. 2015; 1419–1432.

[8] Salmi A, Atzeni E, Iuliano L, Galati M. Experimental Analysis of Residual Stresses on AlSi10Mg Parts Produced by Means of Selective Laser Melting (SLM), in: Procedia CIRP, Elsevier B.V., 2017: pp. 458–463.

[9] Galati M, Iuliano L. A literature review of powder-based electron beam melting focusing on numerical simulations. Addit. Manuf. 2018; 1–20.

[10] Ek RK, Rännar LE, Bäckström M, Carlsson P. The effect of EBM process parameters upon surface roughness. Rapid Prototyp. J. 2016; 495–503.

[11] Galati M, Minetola P, Rizza G. Surface Roughness Characterisation and Analysis of the Electron Beam Melting (EBM) Process. Materials (Basel). 2019; 2211.

[12] Hrabe N, Gnäupel-Herold T, Quinn T. Fatigue properties of a titanium alloy (Ti–6Al–4V) fabricated via electron beam melting (EBM): Effects of internal defects and residual stress. Int. J. Fatigue. 2017; 202–210.

[13] Galarraga H, Warren RJ, Lados DA, Dehoff RR, Kirka MM, Nandwana P. Effects of heat treatments on microstructure and properties of Ti-6Al-4V ELI alloy fabricated by electron beam melting (EBM). Mater. Sci. Eng. A. 2017; 417–428.

[14] Edwards P, O'conner A, Ramulu M. Electron beam additive manufacturing of titanium components: properties and performance. J. Manuf. Sci. Eng. 2013; 61016.

[15] Ali H, Ghadbeigi H, Mumtaz K. Processing Parameter Effects on Residual Stress and Mechanical Properties of Selective Laser Melted Ti6Al4V. J. Mater. Eng. Perform. 2018; 4059–4068.

[16] Galati M, Snis A, Iuliano L. Powder bed properties modelling and 3D thermo-mechanical simulation of the additive manufacturing Electron Beam Melting process. Addit. Manuf. 2019; 100897.

[17] Schajer GS. Practical Residual Stress Measurement Methods, 2013.

[18] Cunningham R, Narra SP, Ozturk T, Beuth J, Rollett AD. Evaluating the Effect of Processing Parameters on Porosity in Electron Beam Melted Ti-6Al-4V via Synchrotron X-ray Microtomography. JOM. 2016;

[19] Todai M, Nakano T, Liu T, Yasuda HY, Hagihara K, Cho K, Ueda M, Takeyama M. Effect of building direction on the microstructure and tensile properties of Ti-48Al-2Cr-2Nb alloy additively manufactured by electron beam melting. Addit. Manuf. 2017;

[20] Biamino S, Penna A, Ackelid U, Sabbadini S, Tassa O, Fino P, Pavese M, Gennaro P, Badini C. Electron beam melting of Ti–48Al–2Cr–2Nb alloy: Microstructure and mechanical properties investigation. Intermetallics. 2011; 776–781.

[21] Murr LE, Gaytan SM, Ceylan A, Martinez E, Martinez JL, Hernandez DH, Machado BI, Ramirez DA, Medina F, Collins S, Wicker RB. Characterization of titanium aluminide alloy components fabricated by additive manufacturing using electron beam melting. Acta Mater. 2010; 1887–1894.

[22] Lin B, Chen W, Yang Y, Wu F, Li Z. Anisotropy of microstructure and tensile properties of Ti–48Al–2Cr–2Nb fabricated by electron beam melting. J. Alloys Compd. 2020; 154684.

[23] Barros R, Silva FJG, Gouveia RM, Saboori A, Marchese G, Biamino S, Salmi A, Atzeni E. Laser powder bed fusion of inconel 718: Residual stress analysis before and after heat treatment. Metals (Basel). 2019;

[24] Salmi A, Atzeni E. Residual stress analysis of thin AlSi10Mg parts produced by Laser Powder Bed Fusion. Virtual Phys. Prototyp. 2020;